ACCSCIENCE PUBLISHING

Explora: Environment and Resource

ORIGINAL RESEARCH ARTICLE

Synergistic effects and mechanism of hazardous chlorinated aromatic hydrocarbon formation during plastics combustion: A multiscale study

Yin Wang[1], Lei Xiong[1], Xingxiang Wang[1], Zehua Huang[2], Jiangbing Li[1]*, and Zhenglei Wu[2]*

[1]Key Laboratory for Green Processing of Chemical Engineering of Xinjiang Bingtuan, School of Chemistry and Chemical Engineering, Shihezi University, Shihezi, Xinjiang, China

[2]Xinjiang Jintai Advanced Materials Technology Co., Ltd, Huyanghe, Xinjiang, China

Abstract

The combustion of waste plastics provides critical insights for researchers addressing environmental challenges. This study systematically investigates the combustion behavior, reaction kinetics, and mechanisms of polypropylene (PP), polystyrene (PS), polyvinyl chloride (PVC), and their ternary blend (PP:PS:PVC). Headspace gas chromatography–mass spectrometry analysis showed that the emitted volatile organic compounds ranged from volatile to semi-volatile regimes, with saturation mass concentrations spanning 0 μg·m^{-3} < $\log_{10}C_0$ < 10 μg·m^{-3}. Co-combustion substantially increased the relative abundance of oxygenated species, such as aldehydes, ketones, esters, and acids, compared with single-component plastics. Two-dimensional correlation spectroscopy indicated that the order of gas evolution was: gaseous acids, residual functional groups, aldehydes, ketones, esters, and, finally, aliphatic hydrocarbons, suggesting premature oxidation in the blend. Iso-conversional kinetic analysis showed that PVC had a significant catalytic effect, reducing the activation energy for PVC dehydrochlorination by approximately 40 kJ·mol^{-1} and for residual carbon oxidation by about 100 kJ·mol^{-1} in the blend compared with pure PVC. Cone calorimetry showed that PS had the highest total smoke release (3,188 m^2·m^{-2}) and PVC produced the highest carbon monoxide yield (0.192 kg·kg^{-1}), indicating a greater hazard. The ternary blend showed an increased carbon monoxide yield of 0.183 kg·kg^{-1} compared with either PP or PS alone. Reactive force field simulations provided atomic-level evidence that PVC-derived chlorine radicals attack PP and PS chains, accelerate radical-driven oxidation, and promote the formation of chlorinated aromatics, such as chlorostyrene (C_8H_7Cl). These findings provide a theoretical basis for developing sustainable strategies for waste plastic combustion and pollution control.

Keywords: Waste plastics; Co-combustion; Chlorine migration; Catalytic synergy; Reaction mechanism; Reactive force field

***Corresponding authors:**
Jiangbing Li
(ljbin@shzu.edu.cn)
Zhenglei Wu
(18530252392@163.com)

Citation: Wang Y, Xiong L, Wang X, Huang Z, Li J, Wu Z. Synergistic effects and mechanism of hazardous chlorinated aromatic hydrocarbon formation during plastics combustion: A multiscale study. *Explora Environ Resour.* 2026;3(2):025480084. doi: 10.36922/EER025480084

Received: November 30, 2025

Revised: February 3, 2026

Accepted: February 3, 2026

Published online: March 27, 2026

1. Introduction

Global plastic production is increasing rapidly due to rising consumer demand, resulting in an unprecedented amount of plastic waste, primarily from single-use items.

When discarded indiscriminately, these materials cause significant pollution and pose serious environmental threats.[1–3] Despite significant efforts to develop new recycling strategies and technologies,[4–6] landfilling and incineration remain the primary methods for managing plastic waste in many low- and middle-income countries. Incineration can reduce plastic waste volume by more than 90%, producing residues that are more suitable for landfilling.[7–10] Additionally, some plastics possess calorific values comparable to or even exceeding those of certain fossil fuels, making them potential energy sources for electricity and heat generation.[11] However, uncontrolled combustion of plastic waste releases substantial amounts of hazardous pollutants, including volatile organic compounds (VOCs), dioxins, polychlorinated biphenyls, and fly ash. These emissions are associated with adverse health effects, such as kidney and liver damage, neurological impairment, and carcinogenicity.[12–15] Therefore, developing effective strategies to detect and mitigate VOCs and other toxic emissions from incineration is essential for advancing sustainable plastic recycling practices.

The incineration of waste plastics is commonly associated with the emission of VOCs and the evolution of residual functional groups (RFGs).[16–18] The analysis of these processes requires advanced techniques, such as thermogravimetry–Fourier transform infrared–mass spectrometry (TG–FTIR–MS) and two-dimensional correlation spectroscopy (2D-COS).[19] For example, Qin *et al.*[20] employed TG–FTIR–MS to examine changes in functional groups and products during the heating of medical plastics, revealing extensive interactions. Building on this work, Liu *et al.*[21] demonstrated that FeAlOx significantly reduced the formation of chlorinated organics in the liquid products during the catalytic thermal degradation of polyvinyl chloride. Subsequently, Wang *et al.*[22] used 2D-COS to investigate the solid-phase contribution to VOCs generation during plastic combustion and identified a four-step process, including dehydration, chain cleavage, and secondary transformation. From an atmospheric perspective, the chemical properties of VOCs, such as saturation mass concentration (C_0), provide essential insights into the complexity and oxygen content of atmospheric organic aerosol.[23,24] Moreover, headspace solid–phase microextraction gas chromatography–mass spectrometry (HS–SPME–GC–MS) has been widely applied to characterize VOC emissions from thermally decomposed waste plastics. Wu *et al.*[25] employed HS–SPME–GC–MS to study the dynamics of VOC emission from microplastics under ultraviolet irradiation and identified numerous hazardous compounds, despite minimal changes in microplastic physicochemical properties. However, although previous studies have focused on reaction kinetics and product identification, critical aspects—such as solid-state reaction mechanisms and the influence of combustion temperature on product distribution—remain inadequately explored. Therefore, an integrated approach combining combustion behavior, product distribution, and reaction mechanisms is imperative to advance the fundamental understanding of plastic combustion processes.

Moreover, obtaining detailed information on intermediate reactions and products through conventional experimental methods remains challenging. Reactive force field molecular dynamics (ReaxFF-MD) simulations have proven particularly effective in capturing bond formation and cleavage events during chemical reactions by utilizing potential energy functions based on bond orders. This technique enables the investigation of reaction mechanisms and dynamic properties throughout combustion processes.[26] For instance, Feng *et al.*[27] employed ReaxFF-MD simulation to study the reaction mechanism and kinetics of cellulose combustion, elucidating the changes of reactants, intermediates, free radicals, and stable product distributions under different conditions, and extracting kinetic parameters for the initial decomposition and subsequent intermediate reactions. Yu *et al.*[28] combined thermogravimetric (TG) analysis with ReaxFF-MD simulations to probe the combustion properties and reaction mechanisms of polyethylene, focusing on the effect of system density on the formation and decomposition of intermediates such as ethylene (C_2H_4). Their results showed that increased polyethylene loading enhanced combustion performance, consistent with dust-ignition results, thereby providing molecular-level insights. Using thermogravimetry–infrared spectroscopy (TG–IR) analysis of polyacrylic ester decomposition products, Saha *et al.*[29] observed that carbon dioxide (CO_2) was generated prior to alkene formation. Corresponding ReaxFF-MD simulations showed that these formation pathways originated from alkoxy bond cleavage and beta (β)-hydrogen elimination, respectively. Furthermore, ReaxFF-MD has been extensively applied to diverse systems, including coal,[30] lignite,[31] and explosives,[32] among others. The integration of advanced experimental techniques with ReaxFF-MD simulations has enabled a better understanding of microscopic reaction mechanisms behind macroscopic phenomena in waste plastic combustion. However, research on the combustion dynamics and mechanisms of multi-component plastic mixtures via ReaxFF-MD simulations remains scarce. A thorough understanding of waste plastic combustion, therefore, necessitates an investigation into the atomic-scale formation and evolution pathways of combustion products.

This study investigates the combustion behaviors of polypropylene (PP), polystyrene (PS), polyvinyl chloride (PVC), and their ternary PP:PS:PVC mixtures, using a combination of experimental techniques and ReaxFF-MD simulations to assess recyclability. Combustion processes and products were characterized by TG–IR, TG–mass spectrometry (TG–MS), *in situ* Fourier transform infrared spectroscopy (FTIR), HS–GC–MS, X-ray photoelectron spectroscopy (XPS), and 2D-COS. Activation energies (E_α) of PP, PS, PVC, and the PP:PS:PVC blend were obtained by TG analysis at different heating rates using the iso-conversional method. Combustion parameters, including total heat release and average effective heat of combustion, were determined using cone calorimetry. Moreover, ReaxFF-MD simulations were performed to understand the microscopic reaction mechanisms underlying the combustion of ternary plastic mixtures at different temperatures. The findings from this study improve our understanding of the combustion mechanisms in PP, PS, PVC, and their mixtures, providing insights that can aid in optimizing heat recovery and the utilization of both single-component and mixed plastic waste.

2. Materials and methods

2.1. Materials

Polypropylene, PS, and PVC powders with a particle size of 13–17 μm were provided by Guangdong Feng Tai Corporation (China). A ternary blend (PP:PS:PVC) was prepared by vertical planetary grinding at 500 rpm for 24 hours. The ternary blend consisted of PP, PS, and PVC in a 1:1:1 mass ratio. To rigorously evaluate potential synergistic effects during the mixed combustion process, a strict control experimental design was used. PP, PS, PVC, and PP:PS:PVC were combusted independently under identical experimental conditions (same sample mass, particle size, heating rate, gas atmosphere, flow rate, and instrument setup). This approach ensured that any observed differences in VOC composition, gas generation curves, reaction kinetics, and combustion toxicity indices could be attributed to chemical interactions among polymer components rather than experimental variability.

2.2. Analysis of volatile organic compounds using TG–FTIR and TG–MS

Volatile organic compounds were analyzed using a thermogravimetric analyzer (Netzsch STA 449 F5, Germany) coupled with an infrared spectrometer (Nicolet IS 50, Thermo Fisher Scientific, United States of America [USA]) and TG analysis coupled with mass spectrometry (TA Instruments/SPT 650+Discovery MS, USA). Approximately 10 ± 0.2 mg of each sample was placed in an alumina crucible and heated from ambient temperature to 600 °C at a heating rate of 10 °C/min under an airflow of 50 mL/min. FTIR spectra were recorded over the range of 600–4,000 cm^{-1} at 8 cm^{-1} resolution. Mass spectrometry was performed in full scan mode with an m/z range of 1–200.

2.3. Observation of combustion process products by HS–GC–MS

Combustion products of the plastic samples were analyzed using a 7697A headspace autosampler coupled with an 8890B gas chromatograph and a 7000D triple quadrupole mass spectrometer (Agilent Technologies, USA), equipped with an electron ionization source operating at 70 eV. Before analysis, samples were molded into uniform shapes to ensure consistent mass and volume. Combustion was initiated using a handheld torch in ambient air, after which the samples were rapidly transferred to headspace vials and sealed. Flame and post-ignition temperatures were measured simultaneously using a portable digital thermometer, while the produced carbon monoxide (CO) and CO_2 concentrations were measured using dedicated gas detectors. For headspace analysis, the sealed vial was shaken at 35 °C for 40 min to capture combustion products and prevent further reactions.[33] Gas chromatographic separation was performed in splitless mode using the following temperature program: initial hold at 35 °C for 6 min, ramping to 300 °C at 10 °C/min, followed by a three-minute hold at 300 °C. Mass spectrometric detection was performed in full-scan mode over an m/z range of 40 to 500, and the spectral data were compared with the National Institute of Standards and Technology database for compound identification. The saturation vapor pressures (p_0) and saturation mass concentration (C_0) values ($\mu g \cdot m^{-3}$) of detected VOC species were subsequently calculated.[34] The C_0 values ($\mu g \cdot m^{-3}$) of plastics–VOCs species were calculated according to Equation 1:

$$C_0 = \frac{M 10^6 p_0}{760 RT} \quad (1)$$

where M is the molar mass ($g \cdot mol^{-1}$), p_0 is the saturation vapor pressure (mm Hg), R is the ideal gas constant (8.205×10^{-5} $atm \cdot K^{-1} \cdot mol^{-1} \cdot m^3$), and T is the temperature (K). The saturation vapor pressure p_0 for each VOC was estimated using the Estimation Programs Interface Suite (version 4.1), averaging the Antoine equation and the modified Grain method. The Antoine equation was used to estimate vapor pressures for compounds with available temperature-dependent vapor–pressure parameters. At the same time, the modified Grain method was applied to structurally similar compounds lacking complete experimental vapor–pressure data. The arithmetic mean of these two estimates was adopted to reduce model bias and uncertainty. This

combined approach has been widely used in atmospheric chemistry and organic aerosol studies to approximate vapor pressures and volatility classes of complex organic compounds. It should be noted that this calculation assumes ideal gas behavior, equilibrium partitioning, and pure compound vapor pressures. Although these assumptions introduce uncertainty for multifunctional oxygenated and chlorinated VOCs, the approach provides a consistent and internally comparable volatility metric for all detected species.

2.4. Investigation of functional groups using XPS, *in situ* FTIR, and 2D-COS

X-ray photoelectron spectroscopy equipped with an Al Kα source (Thermo ESCALAB 250XI, USA) was used to determine the relative amounts of organic chlorine (Cl) in the blend during combustion. The evolution of RFGs during combustion at temperatures between 200 °C and 500 °C was investigated using *in situ* infrared spectroscopy (Bruker INVENIO-S, Germany). Structural transitions at critical temperature intervals were studied. 2D-COS analysis of FTIR data[35–37] was employed to identify relationships and temporal changes between VOCs and RFGs, enabling us to separate overlapping spectral regions. Heterogeneous 2D-COS analysis was performed using infrared spectra of both VOCs and solid residues. Synchronous and asynchronous 2D-COS maps were interpreted according to Noda's rules.[38,39] When peaks or regions in both maps exhibited the same sign, the spectral intensity change at variable v_1 generally occurs before that at v_2; conversely, if the signs were different, the order of the reaction is reversed.[31,35] If the synchronous map signal is zero, the sequential order of intensity changes cannot be determined.[36] Additional methodological details regarding 2D-COS analysis are provided in the Supplementary File.

2.5. Kinetic analysis and cone calorimetry test

Thermogravimetric analysis was conducted at multiple heating rates (10, 15, and 20 °C min^{-1}) under an air atmosphere, with the temperature ramping from ambient to 600 °C. The E_α was determined using iso-conversional methods based on TG data obtained at different heating rates. Comprehensive methodological details on the kinetic analysis are provided in the Supplementary File. Three methods were employed:

(i) Kissinger–Akahira–Sunose (KAS) method[40], as shown in Equation 2:

$$Ln\left(\frac{\beta}{T^2}\right) = Ln\left(\frac{AR}{E_\alpha g(\alpha)}\right) - \frac{E_\alpha}{RT} \quad (2)$$

where E_α was obtained from the slope of $Ln(\beta/T^2)$ vs. $1/T$.

(ii) Flynn–Wall–Ozawa (FWO) method[41], as shown in Equation 3:

$$Ln(\beta) = Ln\left(\frac{AE_\alpha}{Rg(\alpha)}\right) - 5.331 - 1.052\frac{E_\alpha}{RT} \quad (3)$$

where E_α was calculated from the slope of $Ln(\beta)$ vs. $1/T$.

(iii) Starink (STA) method[42], as shown in Equation 4:

$$Ln\left(\frac{\beta}{T^{1.8}}\right) = Ln\left(\frac{AR}{E_\alpha g(\alpha)}\right) - 1.0037\frac{E_\alpha}{RT} \quad (4)$$

where E_α was derived from the slope of $Ln(\beta/T^{1.8})$ vs. $1/T$.

The mean E_α values and standard deviations were reported for each material at conversion degrees (α) ranging from 0.1 to 0.9. The consistency among the three methods was evaluated via linear regression ($R^2 > 0.98$).

A cone calorimeter (Fire Testing Technology Ltd., United Kingdom) was used to characterize the combustion properties of the plastic samples in accordance with ISO 5660. Tests were conducted horizontally for 600 s. Parameters measured included heat release rate, total heat release, mass loss rate, effective heat of combustion, smoke production rate, CO and CO_2 production rates, and ignition time. Samples (100 × 100 × 3 mm^3) were wrapped in aluminum foil, mounted in an edge frame, exposed to a heat flux of 35 $kW{\cdot}m^{-2}$, and tested in triplicate to ensure reproducibility.

2.6. Reactive force field molecular dynamics simulation

Reactive molecular dynamics simulations were performed using the ReaxFF potential within the Large-scale Atomic/Molecular Massively Parallel Simulator (LAMMPS) software package (version 2, April 2025),[43] employing a ReaxFF force field file (Field. Reax. c/h/o/cl) parameterized for C/H/O/Cl elements.[44] The initial configuration, depicted in Figure 1, consisted of a periodic simulation box containing polymer chains with a degree of polymerization of 50 (C_3H_6, C_8H_8, and C_2H_3Cl), and 850 oxygen molecules. The system density was set to $0.1 g{\cdot}cm^{-3}$ to prevent atomic overlap. Before starting the heating protocol, we performed an energy minimization step, followed by equilibration at 300K with a Berendsen thermostat for 10 ps. The system was subsequently maintained at the target temperature. To simulate the combustion process and elucidate reaction pathways as well as the influence of temperature on the combustion of mixed plastics, the system was heated from 300 K to target temperatures of 2,500 K, 3,000 K, and 3,500 K at a constant rate of 20 K/ps, and held at each target temperature for 1,000 ps. All ReaxFF-MD simulations were conducted in the constant number of particles, volume, and energy ensemble, with a time step of 0.1

femtoseconds and a temperature-damping constant of 10 femtoseconds. Previous ReaxFF-MD studies have shown that elevated temperatures have a minimal influence on the underlying reaction mechanisms in hydrocarbon combustion.[43,45–47] Higher simulation temperatures, relative to TG experiments, were selected to access nanosecond time scales and minimize computational cost.

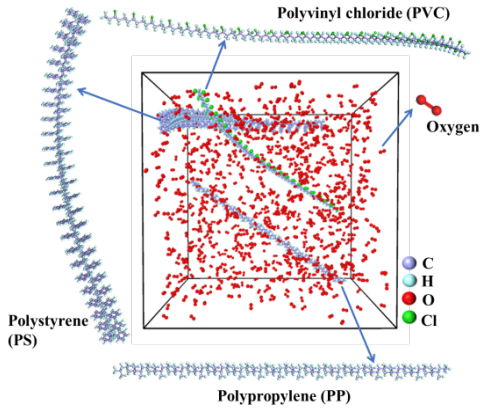

Figure 1. Multi-molecule model of polypropylene: polystyrene: polyvinyl chloride plastic combustion

3. Results and discussion

3.1. Combustion process products and residual solids analysis

3.1.1. Thermogravimetry–infrared spectroscopy analysis

The combustion behaviors of PP, PS, PVC, and their ternary blend were investigated in real time using TG–IR spectroscopy under an air atmosphere. Analysis of the evolved gaseous products, presented as three-dimensional FTIR spectra in Figure 2, revealed distinct differences in the evolution profiles and functional group distributions, highlighting unique combustion mechanisms and potential interactions among the polymers.[48–50]

As shown in Figure 2a, PP combustion is dominated by random chain scission, as evidenced by strong aliphatic C–H stretching around 3,000 cm^{-1}, indicating the release of alkanes and alkenes. This is followed by partial oxidation, reflected by the appearance of C=O bands (1,700–1,750 cm^{-1}; aldehydes, ketones, esters) and C–O vibrations (1,000–1,300 cm^{-1}; ethers, alcohols). Persistent CO_2 (O=C=O near 2,350cm^{-1}) and O–H stretches (3,200–3,600cm^{-1}; water, carboxylic acids) showed progressive oxidation during combustion.[18] Figure 2b shows that PS combustion is characterized by aromatic C–H stretching (3,000–3,100 cm^{-1}) and C=C ring vibrations (1,500–1,600 cm^{-1}), corresponding to the release of styrene (C_8H_8) and other aromatic hydrocarbons. In addition, C=O bands, O–H stretches, and CO_2 absorption near 2,350 cm^{-1} were also observed.[22] PVC had the most complicated two-step degradation (Figure 2c). The first stage was dominated by hydrochloric acid (HCl) release, characterized by broad H–Cl stretching absorption. In the second stage, a pronounced increase in C=O at 1,750 cm^{-1} and O=C=O at 2,350 cm^{-1}, and O–H stretches around 3,600 cm^{-1} was observed, indicating extensive oxidation of the residual char.[51] Finally, the combustion of the ternary blend (Figure 2d) displayed overlapping signals, including aliphatic C–H (2,800–3,000 cm^{-1}) from PP, aromatic C–H and C=C stretching from PS, and the characteristic two-stage release of PVCs. This overlap suggests the coexistence of different routes, as well as possible chemical reactions, such as the catalytic action of PVC-derived HCl on the decomposition of PP and PS.[22] The presence of C=O, O=C=O, and O–H bands indicates the formation of different oxygenated products, which collectively influence the flammability, heat resistance, and emissions characteristics of the blend.

3.1.2. Thermogravimetry–mass spectrometry analysis

While TG–IR provided basic insights into the types of gaseous products produced, TG–MS was employed to determine precisely which new products were formed and how they changed during the heating of PP, PS, PVC, and their ternary blend (Figure 3). From the CO_2 (m/z = 44) evolution profiles (Figure 3a), it can be observed that PP had a sharp, high-intensity peak, indicating efficient combustion. On the contrary, PS had a broad and weak CO_2 release, in line with its predilection for incomplete combustion and soot formation. PVC showed a typical two-step CO_2 release associated with char oxidation after dehydrochlorination. The ternary blend exhibited a non-additive CO_2 release, which is strongly influenced by catalytic interactions among individual polymer degradation products.[52,53] Ion current profiles for some m/z values provided further insights into the degradation mechanisms (Figure 3b,c). Hydrocarbon fragments at m/z 43 and 57 were most abundant for PP due to random chain scission, whereas aromatic fragments at m/z 91 and 104 were most common for PS, indicating depolymerization to styrene. PVC degradation was initiated by dichlorination, as evidenced by the detection of HCl coinciding with the disappearance of the carbon (C)–Cl-related vibration. TG–MS analysis (Figure 3d) shows a strong HCl evolution peak (m/z = 36) at low temperature (around 300 °C) during the first degradation stage of PVC, which is characteristic of dehydrochlorination. HCl is directly released during the initial stage of PVC burning rather than inferred from polymer bond cleavage.[20] Ternary blends exhibited a more complex, multi-step degradation behavior (Figure 3e). In the initial stage, substantial HCl (m/z 36) produced indicates that PVC

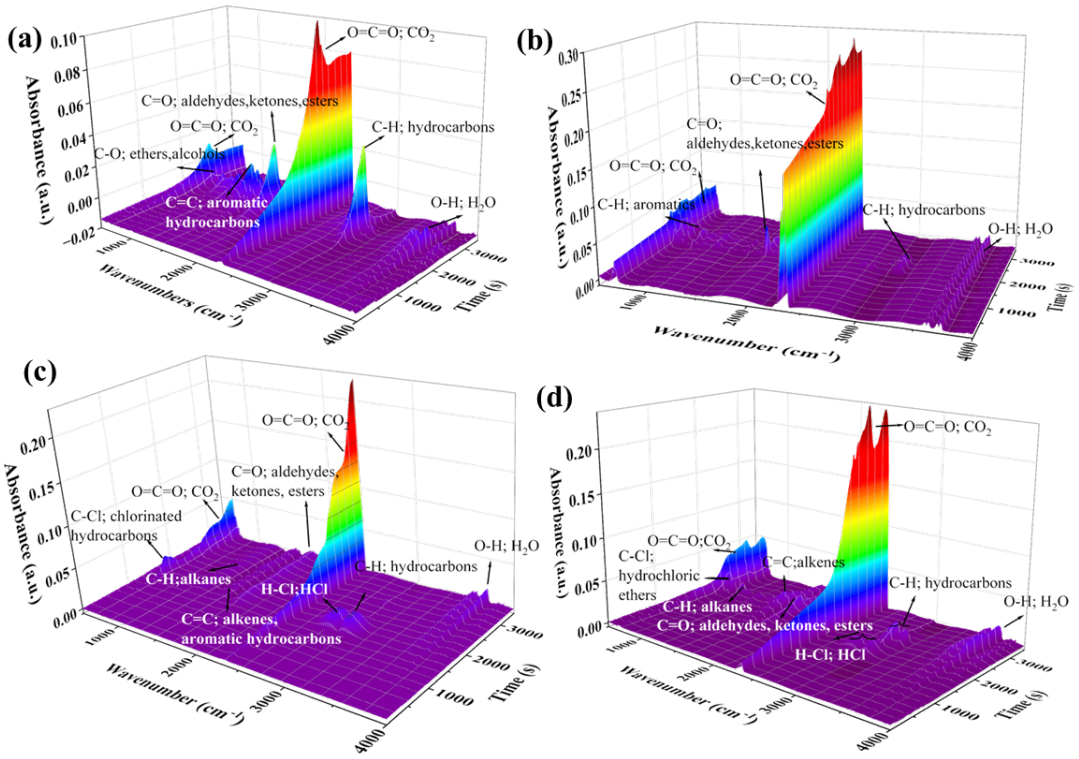

Figure 2. Three-dimensional Fourier transform infrared spectra of volatile organic compounds emitted from the combustion of four types of plastics: (a) polypropylene (PP), (b) polystyrene (PS), (c) polyvinyl chloride (PVC), and (d) PP: PS: PVC

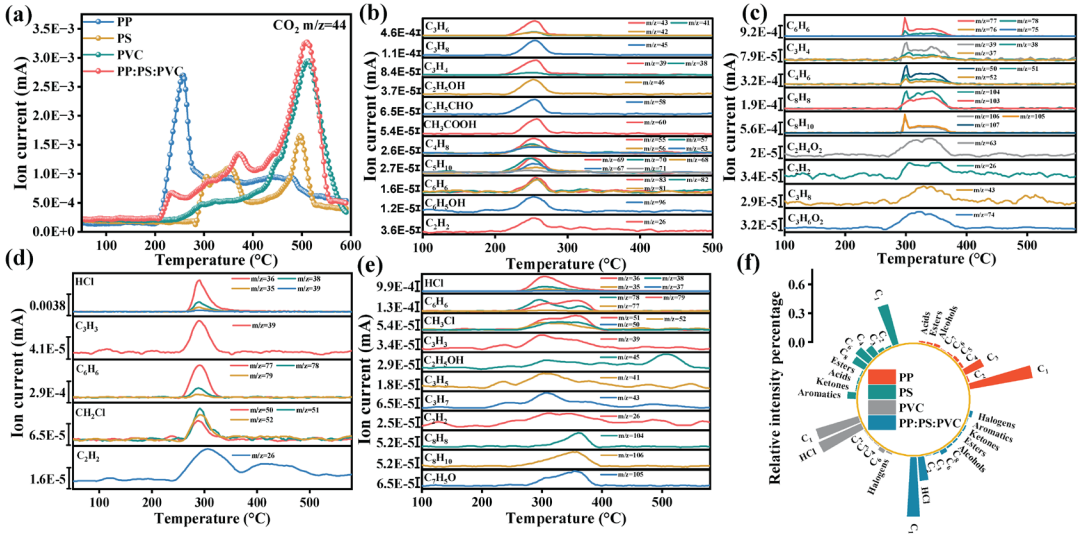

Figure 3. Thermogravimetry–mass spectrometry analysis of gaseous products released during the combustion of the four types of plastics under identical experimental conditions (air atmosphere, heating rate = 10 °C min^{-1}). (a) Evolution of carbon dioxide (m/z = 44) as a function of temperature for polypropylene (PP), polystyrene (PS), polyvinyl chloride (PVC), and PP:PS: PVC. (b–e) Temperature-resolved ion current profiles of representative gaseous fragments detected by mass spectrometry during combustion of (b) PP, (c) PS, (d) PVC, and (e) PP:PS: PVC, respectively. (f) Relative intensity distribution of major volatile organic compounds classes derived from the integrated mass spectrometry signals, including aliphatic hydrocarbons, aromatics, oxygenated compounds (aldehydes, ketones, esters, and acids), and chlorinated species for PP, PS, PVC, and PP:PS: PVC.

degradation dominated the process. Subsequently, aromatic fragments (m/z 78, 104) emerged at approximately 400–450 °C, corresponding to PS decomposition, accompanied by abundant aliphatic bits (m/z 43, 57) derived from PP chain scission. The non-additive blend is characterized by faster CO_2 release and altered product distribution. PVC-derived HCl was inferred to promote the degradation of PP and PS, while secondary reactions generated additional oxygenated (m/z 45, 60) and chlorinated (m/z 50) species, further complicating the volatile profile and highlighting the role of chemical reactions in combustion behavior and emission characteristics.[51] A comparison of relative intensity percentages reveals that (Figure 3f) PP combustion is dominated by a high percentage of CO_2 and low-molecular-weight hydrocarbons, PS degradation is characterized by a distinct dominance of aromatic species, and PVC produces a significant fraction of halogenated species. In contrast, the ternary blend exhibited a more complex and non-additive composition with synergistic effects.[52]

3.1.3. Headspace–gas chromatography–mass spectrometry analysis

Volatile organic compounds released during plastic combustion were sampled and analyzed using HS–GC–MS to identify intermediate products. The relative product content was determined by normalizing chromatographic peak areas.[25]

Compared with the relative amounts of VOCs (Figure 4a), PP mainly contained alkanes and alkenes, consistent with its hydrocarbon structure. PS primarily released aromatic substances due to its benzene ring. PVC produced a more diverse range of products, consisting mainly of alkanes and alcohols, along with substantial amounts of esters, acids, and halogenated compounds. The ternary blend exhibited a composite VOC profile, with a high abundance of alkanes and alcohols, and moderate amounts of esters, aromatics, and acids, indicating that the co-combustion process interacted with and altered the product pathways.[51] The relative percentage composition (Figure 4b) of VOCs further highlights these differences. Specifically, PP combustion products were dominated by alkanes and alkenes. PS degradation was largely characterized by aromatic compounds, and halogenated compounds accounted for approximately 80% of the detected products from PVC. In contrast, the tertiary blend exhibited a composite profile in which halogens, aromatics, and alkanes were the major contributors. Notably, the blend showed a significant increase in oxygenated compounds, such as esters and ketones, in the blend, indicating that chemical reactions occurred during co-combustion and resulted in a more complex product distribution rather than simply the superposition of individual components. Detailed compound information is provided in Table S1. As illustrated in Figure 4c, the identified VOCs displayed a wide volatility distribution with $\log_{10}C_0$ values ranging from approximately 0 to 10 $\mu g \cdot m^{-3}$, encompassing volatile, intermediate-volatile, and semi-volatile organic compounds.[52,53] The relative abundance of VOCs exceeded those reported for coal, wood, and corncob combustion and was comparable to emissions from gas-turbine engines and gasoline vehicles.[54,55] The relationship between $\log_{10}C_0$ and molecular weight indicates that nearly all detected VOCs fell within an established molecular corridor, with linear alkanes at the low-molecular-weight end and alcohols at the higher end. This trend demonstrates a systematic relationship between volatility, molecular size, and function.[56] Analysis of CO and CO_2 release from incomplete combustion in air (Figure 4d) revealed that the ternary blend had the highest absolute CO_2 emission and the largest CO_2/CO ratio among all the blends, implying a possible synergistic effect during co-combustion that promoted more complete oxidation. These findings underscore the significant impact of material composition on combustion efficiency and gas emission profiles.[57] The corresponding flame and sample temperatures are shown in Figure 4e. The temperature profile demonstrates that the external fire source fluctuated between approximately 800 and 850 °C, while all samples maintained a stable thermal response at around 600 °C throughout the combustion process.

3.1.4. X-ray photoelectron spectroscopy and in situ Fourier transform infrared spectroscopy analysis

X-ray photoelectron spectroscopy analysis shows that organic Cl accounts for the majority of the blend's peak area. Upon heating to 400 °C, the surface Cl peak nearly disappeared, indicating the migration of organic Cl during combustion (Figure S1). *In situ* FTIR analysis elucidated the distinct thermal oxidative degradation pathways and the evolution of solid-phase functional groups for PP, PS, PVC, and their ternary blend in air from 200 to 500 °C. For PP (Figure S2a), the intensity of aliphatic C–H stretching vibrations (2,800–3,000 cm^{-1}, from methyl C–H_3 and methylene C–H_2–groups) gradually increased with temperature. Concurrently, emerging bands around 1,710 cm^{-1} (carbonyl C=O in aldehydes, ketones, and carboxylic acids) and 1,600 cm^{-1} (olefinic C=C) indicated oxidative chain scission and the formation of oxygenated intermediates, accompanied by the generation of unsaturated species. The gradual increase of the C–O stretching vibration around 1,200 cm^{-1} was indicative of the formation of ethers, alcohols, esters, and carboxylic acids.[22] PS (Figure S2b) showed very high thermal stability up to 400 °C. It could be seen that there were still aromatic C–H stretching peaks at 3,020 cm^{-1}, and

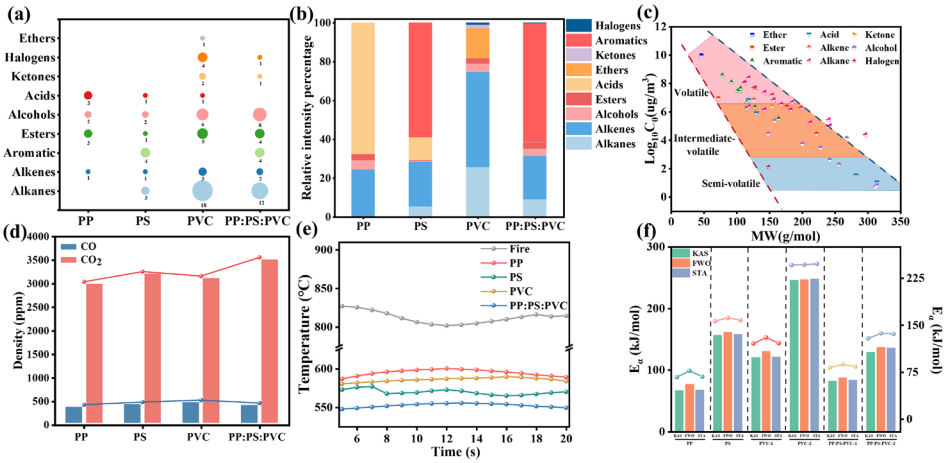

Figure 4. Headspace–gas chromatography–mass spectrometry (HS–GC–MS) analysis of intermediate volatile organic compounds (VOCs) released during combustion of four types of plastics under identical experimental conditions. (a) Distribution of VOC classes identified by HS–GC–MS. The bubble size represents the relative abundance of each VOC class for a given plastic. (b) Relative intensity percentages of major VOC classes for polypropylene (PP), polystyrene (PS), polyvinyl chloride (PVC), and the ternary blend, derived from the integrated HS–GC–MS peak areas. (c) Volatility distribution of individual VOCs as a function of molecular weight (MW) and effective saturation concentration ($\log_{10}C_0$). (d) Ignition and combustion temperatures of PP, PS, PVC, and PP:PS: PVC measured under identical conditions. (e) Relative contents of carbon monoxide and carbon dioxide produced during combustion of the four plastics, reflecting combustion completeness and toxic gas generation. (f) Apparent activation energies of the four plastics obtained using the Kissinger–Akahira–Sunose, Flynn–Wall–Ozawa, and Starink methods.

aromatic ring skeletal vibration peaks at 1,600 cm^{-1} and 1,493 cm^{-1}. Above 400 °C, rapid decomposition occurred, as evidenced by the appearance of broad carbonyl (C=O) and hydroxyl (O–H) bands, indicative of oxidative breakdown of the aromatic backbone.[58] The aromatic C–H stretching bands around 3,000 cm^{-1} showed a strong intensity change at lower temperature (around 200 °C), whereas oxidation-related bands, such as carbonyl C=O stretching around 1,700–1,750 cm^{-1} and hydroxyl O–H stretching around 3,200 cm^{-1}, appeared only at higher temperatures. PVC (Figure S2c) underwent early dehydrochlorination, as shown by the loss of C–H stretching intensity and the appearance of a broad O–H band near 3,000 cm^{-1}. The development of strong carbonyl C=O absorption around 1,700 cm^{-1} and olefinic C=C bands at 1,600 cm^{-1} and across 950–1,650 cm^{-1} was consistent with the formation of conjugated polyene sequences and subsequent oxidized products.[59] Critically, the ternary blend (Figure S2d) displayed a non-additive spectral profile, with accelerated formation of carbonyl and hydroxyl groups at lower temperatures than those observed in the pure polymers. This indicates synergistic interactions during co-combustion, likely mediated by radical cross-reactions that promote oxidation.[57]

3.1.5. Two-dimensional correlation spectroscopy analysis

According to the 2D-COS theory, generalized 2D-COS analysis was performed using TG–FTIR data for VOCs and FTIR data for RFGs, while hetero 2D-COS was conducted using combined TG–FTIR/FTIR datasets for both VOCs and RFGs (Figure 5). The innovative application of two-dimensional TG–FTIR correlation spectroscopy enabled exploration of heterogeneous correlations and sequential temperature responses of evolved VOCs during online plastics combustion (Figure 5a). Synchronous maps revealed distinct centers in various positive auto- and cross-peaks, indicating that most released VOCs changed in the same direction as temperature increased. Compared with single-component systems, the ternary blend exhibited lower intensities in synchronous auto- and cross-peaks, suggesting weaker correlations and minor changes in VOCs. In the asynchronous maps, following Noda's rules,[38] the primary sequential temperature response of VOCs was observed as: acids > aromatics > aldehydes/ketones/esters > aliphatic hydrocarbons > chlorinated hydrocarbons. Detailed response sequences are provided in Table S2. The VOC transformation sequence during the combustion of various plastics is not identical, which may be attributed to differences in their structures and internal reaction pathways. In addition, the compositions of the generated VOCs vary greatly, largely due to differences in polymer backbone structures and the synergistic effects within the mixtures. PS and its blends exhibited a clear tendency toward faster acid production than PP and PVC. First, the inherent structure of PS, in which the instability of the aliphatic carbon attached to the phenyl ring allows rapid oxidative cleavage, resulted in the direct and early formation of benzoic acid derivatives. In the ternary mixture, HCl produced during the early dechlorination reaction of PVC serves as a strong catalyst, greatly

accelerating the oxidation of the intermediate products derived from PP and PS. This allows the oxidation process to proceed beyond typical intermediates, such as alcohols, aldehydes, and ketones, leading to carboxylic acids as the main products. This premature oxidation phenomenon cannot be explained solely by additive effects and thermal decomposition; rather, it reflects accelerated oxidation transformation driven by chemical interactions among polymers. Moreover, VOC evolution is strongly temperature dependent. Emissions mainly occur between 200–500 °C, and the sequential responses within this range are most representative of the overall process. Notably, secondary reactions, such as cracking and oxidation of already formed VOCs into aromatics, hydrocarbons, CO_2, or CO, continue strongly even at high temperatures. In the 2D-FTIR–COS plot (Figure 5b), positive synchronous auto- and cross-regions were observed under an air atmosphere. These synchronous features show that the RFGs associated with hydroxyl, alkane, carbonyl, ketone, aromatic, and fatty ether groups are sensitive to temperature changes and exhibit the same trend direction. Negative synchronous cross-regions in the copolymer RFGs indicate that interactions among components complicate their evolution. In the asynchronous maps, based on Noda's rules,[38] the combustion of PP starts with hydrogen abstraction and peroxide formation, shown by the response of O–H groups. This is followed by backbone scission with the weakening of C–H bonds, and further oxidation to intermediates, such as alcohols and ethers, as indicated by the appearance of C–O bonds. Finally, carbonyl compounds and minor aromatic structures are formed.[22] On the other hand, PS combustion exhibited a unique aromatic-ring-mediated behavior, beginning with cleavage of benzene-ring-derived structures and the aromatic C–H bonds, followed by oxidation and cleavage of the aliphatic side chains, as evidenced by the formation of O–H bonds and a reduction in C–H bonds, leading to oxygen-containing functional groups.[60] PVC combustion is mainly governed by dechlorination, with initial C–Cl bond cleavage and HCl release. The resulting conjugated polyene structures are subsequently oxidized to yield carbonyl compounds, followed by ether bond formation and aliphatic chain breakdown.[61] Notably, the combustion of the ternary blend exhibits substantial synergistic interactions, with both aliphatic chain cleavage and oxidation reactions being significantly accelerated and intensified, as evidenced by enhanced C–H and C–O responses (Table S3). In contrast, the development of aromatic structures is comparatively delayed.

By combining VOCs-FTIR and residual solid FTIR data, heterogeneous 2D-COS provides new insights into the associations between VOCs and solid products during plastic combustion (Figure 5c). Hetero-synchronous maps show broad negative and positive regions, indicating that most gas–solid products exhibit either opposite (generation versus degradation) or identical (synchronous formation) trends. The hetero-asynchronous signals of each plastic are generally consistent with their corresponding hetero-synchronous signals across specific wavelength ranges, demonstrating that temperature responses of most identified RFGs typically precede those of the identified VOCs.[61] According to Noda's rules,[38] the sign relationships between the cross-peaks of aromatic C–H bands and oxidation-associated bands (C=O and O–H) indicate that the spectral intensity changes of aromatic C–H bonds precede those of carbonyl and hydroxyl groups (Figure 5d). This establishes that the initial combustion stage of PS and the PS-containing blend is dominated by aromatic ring-related bond cleavage and side-chain dissociation, followed by oxidative functionalization. A sequential temperature response was observed as: gaseous acids/aromatics > almost identified RFGs > gaseous aldehydes/ketones/esters > gaseous aliphatic hydrocarbons (Table S4), suggesting that high temperatures drive the degradation of functional groups into hydrocarbons. These hydrocarbons subsequently undergo oxidation to produce small molecules such as CO, CO_2, and water (H_2O). Critically, the ternary blend exhibits non-additive properties. When hydrogen chloride is released from PVC, it catalyzes the oxidation of PP and PS in the blend, accelerating carboxylic acid formation and altering aromatic compound evolution. Such catalytic cross-reactions modify the combustion mechanism and product distribution, indicating that the combustion behavior of mixed plastic waste cannot be predicted solely from that of individual polymers burned separately.[57]

3.2. Combustion kinetics and combustion characteristic analysis

3.2.1. Combustion behavior

Thermogravimetric analyses of the four plastics were conducted at heating rates of 10, 15, and 20 °C min^{-1} under an air atmosphere (Figure 6). Increasing the heating rate shifted both the initial decomposition temperature and the temperature of maximum mass loss to higher values, a phenomenon attributed to thermal hysteresis.[62] PP, with its hydrocarbon backbone, underwent a single degradation step, which mainly occurred between 300 and 400 °C. PS, due to its aromatic side-group structure, decomposed over a higher temperature range of approximately 380–400 °C and produced minimal residue. In contrast, PVC underwent a two-stage degradation: the first mass loss (200–400 °C) was attributed to dehydrochlorination, while the second stage (above 400 °C) was associated with

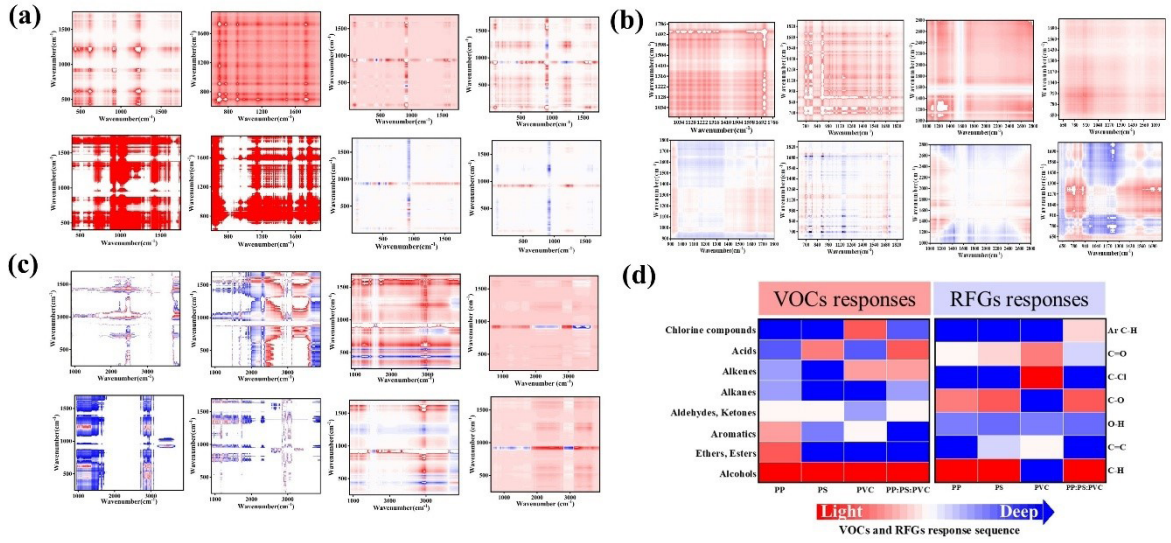

Figure 5. Two-dimensional correlation spectroscopy (2D-COS) analysis reveals the temperature-dependent relationship between evolved volatile organic compounds (VOCs) and residual functional groups (RFGs) during the combustion of plastics. Temperature was used as the external perturbation variable to construct the 2D-COS maps. (a) Synchronous and asynchronous 2D-COS maps of VOCs derived from thermogravimetry–Fourier transform infrared spectroscopy spectra, illustrating correlated intensity variations and sequential changes of characteristic gaseous functional groups as a function of temperature. (b) Synchronous and asynchronous 2D-COS maps of RFGs in the condensed phase, reflecting temperature-induced transformations of surface functional groups on solid residues. (c) Hetero-2D-COS maps correlating VOCs and RFGs, highlighting cross-correlations between gas-phase species evolution and solid-phase functional group changes. (d) Summary heatmap of the sequential temperature responses of major VOC classes for polypropylene, polystyrene, polyvinyl chloride, and the ternary blend. In the synchronous and asynchronous maps, red and blue colors represent positive and negative correlations, respectively.

cleavage of the carbon backbone. The effects of heating rate on mass-loss behavior and residual char formation indicate that heat transfer and reaction kinetics jointly affect the degradation process.[56]

3.2.2. Kinetic analysis

Based on the TG data, kinetic parameters of the four plastics were obtained to better understand their burning behaviors and to provide a theoretical basis for practical applications. Various iso-conversional models, such as KAS, FWO, and STA, were used to determine the E_α. E_α values at different conversion degrees (α = 0.1–0.9), which were estimated from the slope of the fitted line, are summarized in Figure S3. E_α represents the energy barrier of the reaction; lower E_α values indicate that pyrolysis occurs more readily. As shown in Figure 4f, the E_α values obtained from the FWO, KAS, and STA methods are nearly identical, with high average correlation coefficients (R^2 > 0.98; Table S5), demonstrating the consistency and reliability of the kinetic analysis. PP showed single-stage degradation behavior, with apparent E_α values in the range of approximately 66–76 kJ·mol^{-1}. PS underwent single-stage degradation but with a much higher E_α range of 156–161 kJ·mol^{-1}, consistent with the enhanced stability imparted by its aromatic structure. PVC underwent two distinct degradation stages characterized by a relatively low E_α for the initial dehydrochlorination reaction (120–130 kJ·mol^{-1}) and a much higher E_α for the subsequent carbon-chain cleavage (245–250 kJ·mol^{-1}). The ternary blend showed great synergistic effects during degradation. HCl released from PVC decomposition strongly catalyzed the degradation of PP and PS, leading to earlier mass-loss stages and altered reaction pathways. Incorporation of PP and PS reduced the E_α of PVC degradation to 87–80 kJ·mol^{-1} and 136–128 kJ·mol^{-1} for the first and second stages, respectively, indicating facilitated degradation in the multicomponent system.[57] These kinetic results provide quantifiable evidence of the complex interactions that occur during the combustion of mixed plastics.

3.2.3. Combustion characteristics

The combustion characteristics of the four plastics were further studied using a cone calorimeter for 600 s. Parameters such as the heat release rate (HRR), peak heat release rate (PHRR), total heat release (THR), total smoke release, and average effective heat of combustion provided a comprehensive evaluation and forecast of plastic burning behavior.[63,64] As shown in Table 1 and Figure 7a,b, the combustion behavior of these four plastics differs markedly. PS exhibited the highest fire risk, with a PHRR of approximately 720 kW·m^{-2} and the highest THR at 95 MJ·m^{-2}, indicating rapid and intense burning. PP displayed

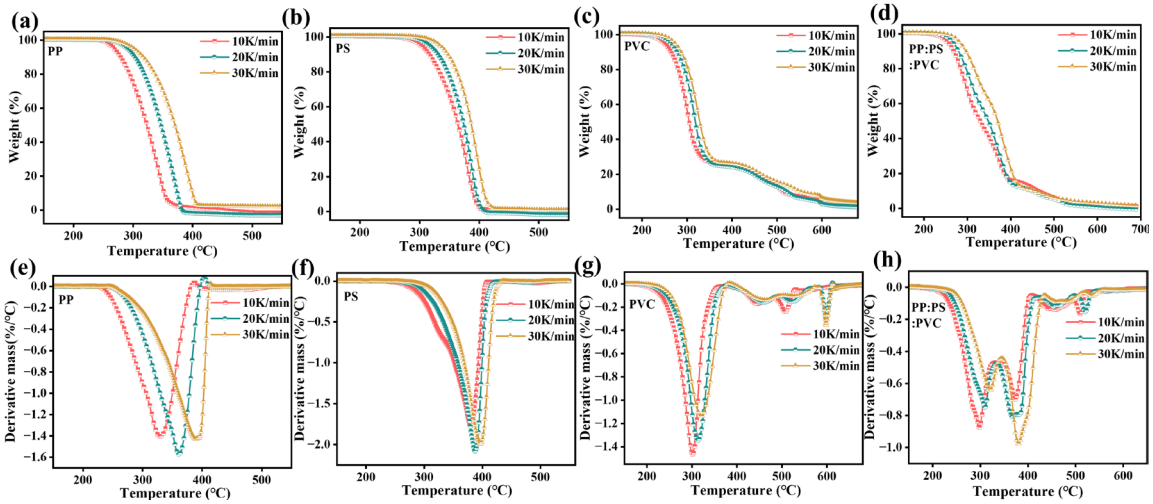

Figure 6. Thermogravimetry (TG) and derivative thermogravimetry (DTG) curves of polypropylene (PP), polystyrene (PS), polyvinyl chloride (PVC), and PP:PS:PVC at different heating rates (10, 15, and 20 °C·min^{-1}) under an air. (a–d) TG curves indicating the mass-loss behavior of (a) PP, (b) PS, (c) PVC, and (d) the ternary blend with respect to temperature. (e–h) Corresponding DTG curves representing the rate of mass loss for (e) PP, (f) PS, (g) PVC, and (h) the ternary blend.

a wider HRR curve, with a PHRR of about 650 kW·m^{-2} and a THR of 84 MJ·m^{-2}, corresponding to a continuous but less intense combustion. PVC showed a relatively flat HRR curve, with the lowest PHRR (~220 kW·m^{-2}) and THR (~50 MJ·m^{-2}), consistent with smoke-dominated, inefficient combustion. The ternary blend exhibited intermediate PHRR (~600kW·m^{-2}) and THR (~22 MJ·m^{-2}) values, indicating that PVC partially reduced PS's main effect on overall combustibility. As shown in Figure 7c, substantial smoke release occurred during the first 0–200 s of burning, indicating that the majority of smoke was emitted during the flaming combustion stage. PS produced the greatest total smoke release due to its aromatic rings, resulting in considerable soot formation during combustion. In contrast, PP, as a saturated hydrocarbon, underwent nearly complete combustion and produced minimal smoke. The ternary blend showed synergistic effects,[57] with smoke production significantly higher than that from PP or PVC burned separately. PVC posed the highest toxicity risk, with a peak CO concentration of 500 ppm (Figure 7d), likely due to Cl inhibition of incomplete combustion. It also had the lowest CO_2 release at 5,400 ppm (Figure 7e) and the highest residual char, indicating inefficient, smoky combustion. On the contrary, PS exhibited the most efficient combustion, with the highest CO_2 release of 19,800 ppm and nearly complete mass consumption (98% mass loss, Figure 7f), consistent with its high flammability. PP showed moderate CO_2 release and 95% mass loss. The ternary blend exhibited intermediate, synergistic behavior, with CO release reaching 780 ppm, considerably higher than either PP or PVC alone. Collectively, these results indicate that PS is the dominant factor controlling the amount of smoke and char formation in the blend.

Table 1. The combustion characteristics of four types of plastics were measured using a cone calorimeter

Parameters	PP	PS	PVC	PP:PS:PVC
Time to ignition (s)	44.000	56.000	26.000	45.000
Peak heat release rate (kW·m^{-2})	723.702	831.183	268.065	693.762
Time to PHRR	126.000	97.000	60.000	102.000
Average to HRR	165.470	169.630	89.090	151.778
Total heat release (MJ·m^{-2})	97.241	109.696	58.609	87.349
Average effective heat of combustion (MJ·kg^{-1})	31.497	24.963	17.384	29.530
Total smoke release (m^2·m^{-2})	569.929	3,188.278	2,179.801	2,646.401
CO yield (kg·kg^{-1})	0.065	0.078	0.192	0.183
CO_2 yield (kg·kg^{-1})	7.834	6.428	5.814	9.727

Abbreviations: CO: Carbon monoxide; CO_2: Carbon dioxide; PP: Polypropylene; PS: Polystyrene; PVC: Polyvinyl chloride.

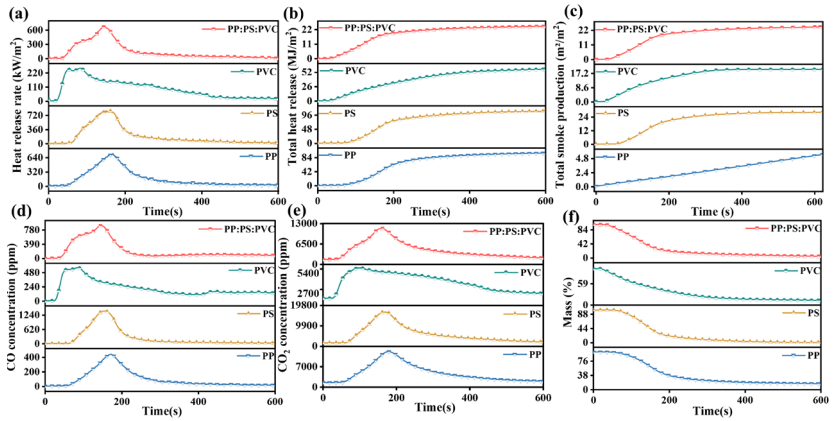

Figure 7. The combustion process characteristics of four types of plastics as measured by the cone calorimeter. (a) Heat release rate. (b) Total heat release. (c) Total smoke production. (d) Carbon monoxide (CO) concentration. (e) Carbon dioxide (CO_2) concentration. (f) Mass loss.
Abbreviations: PP: Polypropylene; PS: Polystyrene; PVC: Polyvinyl chloride.

3.3. Reaction pathways and chlorine migration mechanisms

3.3.1. Distribution of main products under different temperature systems

The quantitative development of the main products generated during the combustion of the three-component plastic blend at different simulation temperatures is shown in Figure S4. The temporal dynamics of oxygen consumption (Figure S4a) show that the reaction was initiated at approximately 200 ps and reached a steady state at around 1,000 ps. At 2,500 K, approximately 50 oxygen molecules were consumed. This number increased to around 200 molecules at 3,000 K and ultimately reached complete consumption of all 550 oxygen molecules at 3,500 K. The formation profiles of the major combustion products—CO_2, CO, and H_2O—are shown in Figure S4b–d. At 2,500 K, these species appeared at approximately 640, 605, and 310 ps, respectively. As the temperature increased to 3,000 K, their formation was accelerated, with appearance times shifting to about 410, 400, and 300 ps. At 3,500 K, these products formed were close to 200 ps, and their final yields were significantly higher than those at lower temperatures. Figure S4e,f shows substantial early-stage production of C_8H_8 and propylene (C_3H_6), identified as the main thermal decomposition products of PS and PP, respectively. Their concentrations peaked below 200 ps and subsequently decreased as they were consumed in secondary reactions to form other species, such as chlorostyrene (C_8H_8Cl) and C_2H_4. The generation of HCl and hydrogen (H_2) was minimal at 2,500 K but increased steadily at 3,000 K and 3,500 K. Both species stabilized at approximately 110 ps, with hydrogen chloride appearing earlier than H_2 (Figure S4g,h). Hydrogen chloride mainly originated from the decomposition of chloroethylene (C_2H_4Cl). Additionally, chloroethene (C_2H_3Cl), produced predominantly through the thermal degradation of PVC, appeared at around 125 ps at all temperatures (Figure S4i). Similar to C_8H_8 and C_3H_6, its yield exhibited a typical rise-and-fall pattern with increasing simulation time, with the final yield increasing with temperature. C_2H_4, mainly derived from PP chain reactions, began to be consumed after 600 ps at 3,500 K. The $\cdot HO_2$ radical, a key intermediate of the oxidation process, ultimately contributed to the formation of CO and CO_2. Benzene (C_6H_6), primarily formed through the decomposition of C_8H_8, increased in abundance with temperature, indicating that higher temperatures accelerate combustion reactions by enhancing molecular motion, thereby promoting reaction rates and product formation.[65]

3.3.2. Chlorine distribution and reaction mechanism during combustion

Consistent with previous studies and the present experimental results, ReaxFF-MD simulation showed that temperature primarily controls reaction rates and product yields, while the fundamental product types and reaction pathways remain unchanged. To clarify these pathways, product evolution was studied at 2,500 K. The simulations describe the combustion process of a PP:PS:PVC ternary blend in the presence of an oxygen atom, capturing the complete reaction chain from macromolecule polymers to small gaseous molecules through bond cleavage, rearrangement, and oxidation reactions.[66]

The detailed reaction sequence at 2,500 K is shown in Figure 8. The initiation stage began with the dissociation of an ethylbenzene (C_9H_{10}) aromatic fragment from PS at 89 ps, followed by substantial formation of C_8H_8 at 99 ps and the appearance of the benzyl radical ($\cdot C_7H_7$) at 130.7 ps. Simultaneously, rapid dechlorination of PVC occurred:

C_2H_3Cl was detected at 125.3 ps, and hydrogen chloride at 198.1 ps. This sequence is consistent with a free-radical chain mechanism initiated by the breaking of the C–Cl bond in PVC. At 113.2 ps and 125.1 ps, C_3H_6 and C_2H_4 were detected, respectively. The appearance of $\cdot HO_2$ at 143.2 ps indicates that small-molecule formation occurred early through segmental reactions during macromolecular chain combustion. The formation of chlorinated benzyl radical (C_8H_7Cl) at 151.3 ps provides direct proof of the synergistic catalytic effect of ·Cl, showing their addition to C_8H_8 derived from PS. Key oxygenated intermediates of the oxidation process, including formylperoxy radical (C_2HO_2), ketene (C_2H_2O), acetylene (C_2H_2), formic acid (CH_2O_2), and formaldehyde (CH_2O), were identified. These intermediates have also been observed in coal–oxygen combustion experiments and in ReaxFF studies of cellulose and cellobiose combustion[27], supporting the reliability of the reaction pathways identified in this study. Reactive radicals such as ·H, hydroxyl (·OH), and hydroperoxyl ($\cdot HO_2$) participated actively in both the consumption and production of different intermediates. At 175 ps, the formyl radical (·CHO), an important precursor for aldehyde decomposition and a main source of CO, was detected. H_2O, detected at 310 ps, primarily formed through a combination of ·H and ·OH radicals, whereas after 428.5 ps, most H_2 originated from hydrogen abstraction from C_3H_6. CO and CO_2 were detected at 605.7 ps and 640.1 ps, respectively, indicating that they are end products of advanced oxidation. C_6H_6 appeared later, around 781.4 ps, due to its highly stable conjugated structure and a complex multistep formation process. The primary route observed in the trajectory involved direct release of styrene from PS via C–C bond cleavage in the aromatic side chain, followed by dehydrogenation to benzene. A secondary, kinetically slower pathway involved the cyclization and aromatization of smaller fragments (e.g., alkenes and alkynes) and required a high activation energy. Additionally, early-stage release of Cl species from PVC consumed carbon sources through competitive reactions, indirectly delaying the benzene formation window. Based on these observations, a multi-stage reaction model is proposed: (i) initiation via PVC dichlorination, (ii) PP and PS chain scission, (iii) Cl-catalyzed oxidation, and (iv) formation of small molecular products. This sequence of key intermediates is consistent with the conclusions derived from the 2D-COS analysis.

Based on the identified reaction pathways, the general combustion process of the mixed plastic is shown in Figure 9. The initial reaction phase is characterized by the low-energy-barrier cleavage of C–Cl bonds in PVC, resulting in highly reactive ·Cl. These radicals act as efficient initiators, rapidly attacking the molecular chains of PP and PS via hydrogen abstraction to generate alkyl and aryl radicals, thereby drastically accelerating the dissociation

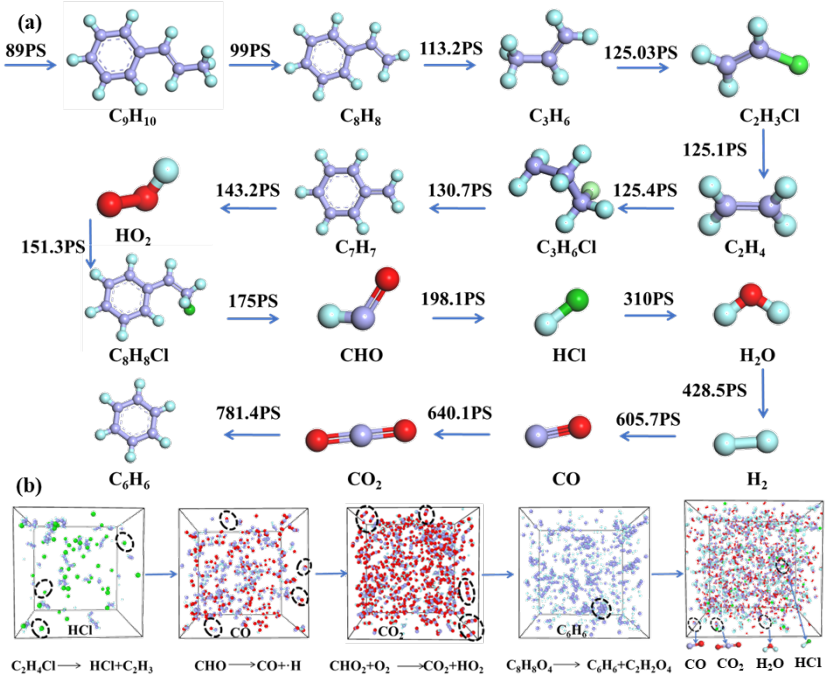

Figure 8. The main product formation and reaction pathways of the mixed plastic combustion process were simulated using reactive force field–molecular dynamics at 2,500 K. (a) Main product formation pathways. (b) Reaction pathways.

of the entire blend system. PP predominantly decomposes through β-scission, producing C_3H_6 and other short-chain olefins, whereas PS undergoes C–C bond cleavage in its aromatic side chains, releasing styrene and benzyl radicals. In the presence of oxygen, these radicals readily undergo oxidation. Alkyl radicals react with O_2 to form peroxy radicals, which then rearrange and undergo β-scission to yield key oxygenated intermediates such as aldehydes, ketones, and small carboxylic acids. Cl-containing species released from PVC play a critical role in triggering those oxidation reactions. The presence of ·Cl and HCl promotes the cleavage of peroxy bonds and selectively directs reactions toward the formation of aldehydes and CO. The evolution of aromatic products is more complex. Styrene and benzene generated from PS depolymerization can undergo electrophilic attack, leading to aromatic ring opening and subsequent oxidation. Ultimately, these processes produce small molecular acids, such as carboxyl radicals ($\cdot CHO_2$), and release CO_2 through a series of decomposition and recombination steps. Simultaneously, the addition of ·Cl to aromatic rings yields chlorinated aromatics (e.g., C_8H_7Cl), with the final gaseous product arising from multiple competing pathways. CO is primarily produced through the rapid decomposition of aldehyde groups, especially the ·CHO moiety, whereas CO_2 mainly originates from the decarboxylation of $\cdot CHO_2$ and the deep oxidation of acid intermediates ($\cdot CHO_2 + O_2 \rightarrow CO_2 + \cdot HO_2$, $\cdot CHO_2 \rightarrow CO_2 + \cdot H$). H_2 formation results from radical recombination and hydrocarbon dehydrogenation at high temperature. Overall, the main driving force underlying these complex reaction networks is the highly effective chain reaction initiated by ·Cl radicals. This catalytic synergy substantially lowers the activation energy of oxidation reactions.[58] This mechanistic understanding provides key theoretical insights into pollutant formation during the co-combustion of complex waste plastics. In the context of recent development of carbon dot–polymer hybrid composites, there is an increasing demand for a detailed understanding of polymer degradation, oxidation, and interfacial chemistry under thermal and oxidative conditions, which is closely linked to the combustion and thermal stability mechanisms elucidated in this study.[67]

3.4. Implications for life cycle and techno-economic performance

Although the present study primarily focuses on combustion behavior, pollutant formation mechanisms, and Cl-driven synergistic effects at the molecular and process scales, the results also have important implications for life cycle assessment (LCA) and techno-economic analysis (TEA) of waste plastic incineration systems.

To provide a quantitative perspective relevant to LCA and TEA, a first-order direct carbon footprint was estimated from the cone calorimeter emission yields (Table 1). This estimate assumes complete atmospheric oxidation of CO to CO_2. The CO-derived CO_2-equivalent mass was calculated as Equation 5:

$$m_{CO_2\text{-eq},CO} = m_{CO} * \frac{44}{28} \quad (5)$$

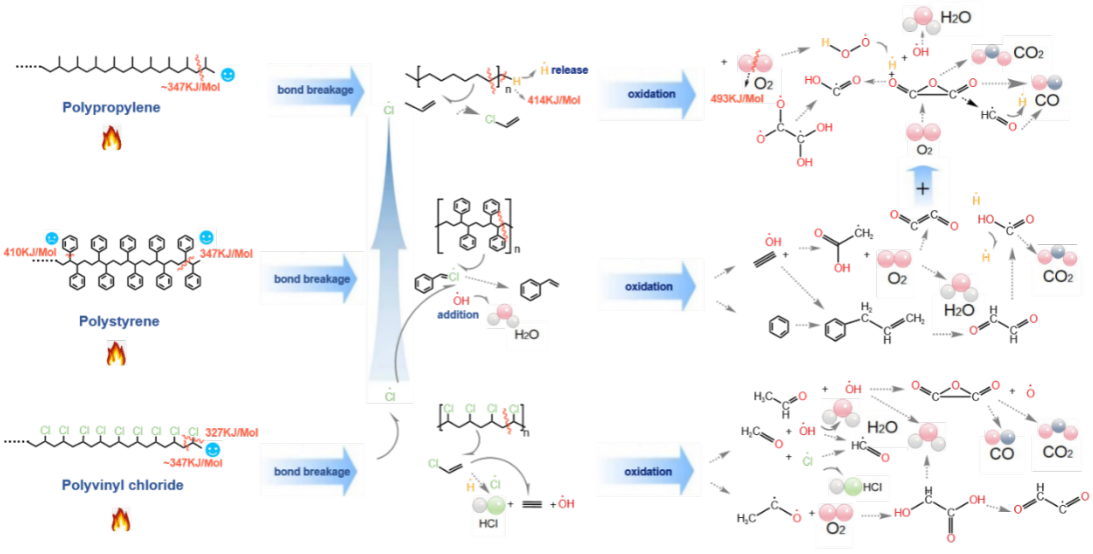

Figure 9. General combustion mechanism of polypropylene: polystyrene: polyvinyl chloride proposed based on reactive force field–molecular dynamics simulations

The first-order direct carbon footprint was then defined as Equation 6:

$$CF_{direct}=m_{co_2}+m_{co}*\frac{44}{28} \quad (6)$$

where m_{CO2} and m_{CO} are the experimentally determined CO_2 and CO yields in kg·kg^{-1} fuel. To enable comparison on an energy recovery basis consistent with LCA inventory modeling, the carbon footprint intensity was normalized by the effective heat of combustion (EHC) (Equation 7):

$$CF_{MJ}=\frac{CF_{direct}}{EHC} \quad (7)$$

where *EHC* is expressed in MJ·kg^{-1}.

The ternary blend exhibited a significantly higher direct carbon footprint ($CF_{direct}=10.014\text{kg CO}_2-\text{eq kg}^{-1}$) than PP (7.936), PS (6.550), and PVC (6.116). When normalized by energy recovery, the ternary blend showed a carbon-footprint intensity of $CF_{MJ}=0.339\text{kg CO}_2-\text{eq MJ}^{-1}$, which is markedly higher than PP (0.252) and PS (0.263), and comparable to the high-intensity level of PVC (0.352). This indicates a high climate load per unit of recovered energy, attributable to Cl-driven incomplete combustion, as evidenced by the substantially elevated CO production in the ternary system.

To test whether the environmental burden of the ternary blend can be approximated by linear superposition of single-component inventories, an additive (no-synergy) baseline was constructed for a 1:1:1 mass ratio of PP:PS:PVC, as shown in Equation 8:

$$X_{add}=\frac{X_{PP}+X_{PS}+X_{PVC}}{3} \quad (8)$$

where (*X*) represents any emission or performance indicator, such as CO_2 yield, CO yield, *EHC*, and (CF_{direct})

The dimensionless synergy factor is defined as Equation 9:

$$SF_X=\frac{X_{measured}}{X_{add}} \quad (9)$$

where ($X_{measured}$) is the experimentally measured value for the ternary blend.

Using this framework, the additive baseline carbon-footprint intensity was calculated as ($CF_{MJ,\,add}=0.279\text{ kg CO}_2\text{-eq MJ}^{-1}$), whereas the measured value for the ternary blend was $0.339\text{ kg CO}_2-\text{eqMJ}^{-1}$, yielding a synergy factor of $SF_{CF_{MJ}}=1.22$. Similarly, the synergy factors for CO_2 and CO yields were 1.45 and 1.64, respectively, indicating a substantial increase in greenhouse gas emissions and incomplete combustion products induced by Cl interactions.

In addition to carbon emissions, acid gas release—primarily HCl—introduces significant downstream pollution control requirements, affecting both operating costs (TEA) and indirect life-cycle emissions. Under a conservative upper-bound assumption that all Cl in PVC is quantitatively released as HCl, the theoretical maximum mass fraction of HCl generated from PVC is approximately 56 wt.%.[68] For a 1:1:1 PP:PS:PVC blend, the maximum HCl generation per unit mass of fuel is as shown in Equation 10:

$$m_{HCl,\,max}=0.56*\frac{1}{3}=0.1867\text{ kg}_{HCl}\text{kg}^{-1}{}_{blend} \quad (10)$$

The corresponding molar amount of HCl is shown in Equation 11:

$$n_{HCl}=\frac{1000*m_{HCl,\,max}}{36.46}=5.12\text{ mol kg}^{-1}{}_{blend} \quad (11)$$

Assuming a typical engineering design Ca/Cl molar ratio of 2:1 for dry or semi-dry flue-gas treatment, the theoretical CaO consumption is shown in Equation 12:

$$m_{CaO}=2*n_{HCl}*\frac{56.08}{1000}=0.574\text{ kg}_{CaO}\text{kg}^{-1}{}_{blend} \quad (12)$$

Normalized by energy recovery, the CaO demand becomes Equation 13:

$$m_{CaO,\,MJ}=\frac{m_{CaO}}{EHC_{Ternary}}=\frac{0.574}{29.530326}=0.0194\text{ kg}_{CaO}\text{MJ}^{-1} \quad (13)$$

This additional reagent demand increases operating costs and indirect energy-related carbon emissions, worsening both LCA and TEA outcomes. Collectively, these simplified estimates show that PVC-driven synergistic chemistry alters the process outcomes, amplifying the direct carbon footprint and increasing the downstream pollution control burden in mixed plastic combustion systems.

4. Conclusion

In this study, we elucidated the formation mechanisms of hazardous chlorinated aromatic hydrocarbons and VOCs during the co-combustion of PVC with PP and PS. Multiscale experiments and analyses combined with ReaxFF-MD simulations showed that the combustion behavior of PVC-containing blends is not a simple additive effect but is strongly influenced by noticeable synergistic effects. These interactions substantially alter the emission characteristics and environmental impact, with Cl's catalytic role identified as the main hazard. At

the atomic scale, ReaxFF-MD simulations revealed that ·Cl radicals generated from PVC decomposition actively attack the hydrocarbon chains of PP and PS, significantly accelerating their oxidative degradation. This catalytic cycle lowers the E_α and promotes the rapid formation of harmful chlorinated aromatic species. Macroscopically, it results in an altered product distribution, with early and elevated formation of oxygenated VOCs and carboxylic acids, as captured by 2D-COS.

From an environmental impact perspective, the hazardous compounds identified, mainly chlorinated aromatic hydrocarbons and oxygen-containing volatile organic compounds (aldehydes, ketones, esters), pose multiple ecological and health risks. First, their semi-volatile properties (saturation mass concentration $\log_{10}C_0$ ranging from 0 to 10 μg·m^{-3} and spanning both volatile and semi-volatile regimes) enable long-range atmospheric transport and prolonged persistence in water bodies and soil following deposition. Second, the chlorinated structure of chlorinated aromatic hydrocarbons confers high ecological toxicity. Similar to persistent organic pollutants such as dioxins, these compounds can bioaccumulate through the food chain, posing serious threats to aquatic organisms and terrestrial ecosystems. Cone calorimeter results further indicate that the CO produced by ternary mixed combustion (0.183 kg·kg^{-1}) is much higher than that from individual plastics (TSR = 2,646 m^2·m^{-2}), accompanied by synergistically increased smoke production. These incomplete combustion products directly impair respiratory health and also contribute to surface ozone formation through photochemical reactions, thereby exacerbating photochemical smog. The ReaxFF-MD simulation pathway also shows that the chlorinated aromatic compound (C_8H_7Cl) produced by the catalytic effect of ·Cl radicals is environmentally persistent and resistant to degradation. Therefore, pre-treatment of PVC or the incorporation of Cl scavengers is essential to inhibit the formation pathways of these high-risk compounds, thereby reducing their long-term cumulative risks to the environment and public health.

Acknowledgements

The authors thank the Key Laboratory for Green Processing of Chemical Engineering of Xinjiang Bingtuan for providing the necessary facilities and support during this study.

Funding

The work was supported by the Science and Technology Program of XPCC (No.2023AB032, No. 2025DA005, No.2025DA047), and the Scientific and Technological Innovation Leading Talent of Tianchi (No. CZ002703).

Conflict of interest

Zehua Huang and Zhenglei Wu are employees of Xinjiang Jintai Advanced Materials Technology Co., Ltd. The authors declare no other competing interests beyond the relationships stated above.

Author contributions

Conceptualization: Yin Wang, Xiong Lei, Jiangbing Li
Formal analysis: Yin Wang, Xingxiang Wang
Investigation: Yin Wang
Methodology: Jiangbing Li
Project administration: Zehua Huang, Jiangbing Li
Supervision: Xiong Lei, Jiangbing Li
Validation: Xingxiang Wang
Writing–original draft: Yin Wang
Writing–review & editing: Xiong Lei, Zehua Huang, Zhenglei Wu, Jiangbing Li

Ethics approval and consent to participate

Not applicable.

Consent for publication

Not applicable.

Availability of data

Data will be made available upon reasonable request to the corresponding author. Additional data associated with this article can be found in the Supplementary File.

References

1. Aransiola SA, Victor-Ekwebelem MO, Daza BX, *et al*. Micro- and nano-plastics pollution in the marine environment: Progresses, drawbacks and future guidelines. *Chemosphere*. 2025;374:144211.

   doi: 10.1016/j.chemosphere.2025.144211

2. Guan J, Dai Z, Wang R, *et al*. Pollution characteristics and control strategies of typical waste plastic recycling plants. *J Environ Chem Eng*. 2025;13(3):116398.

   doi: 10.1016/j.jece.2025.116398

3. Yan Y, Wang Y. Boosting bioplastics' discovery for curbing plastic pollution. *Matter*. 2025;8(7):102167.

   doi: 10.1016/j.matt.2025.102167

4. Ryou H, Byun J, Bae J, Kim DK, Han J. Energy-efficient and environmentally friendly upcycling of waste plastic into fuels, chemicals, and polymers. *Chem Eng J*. 2025;511:162256.

   doi: 10.1016/j.cej.2025.162256

5. Xu S, Han Z, Yuan K, *et al*. Upcycling chlorinated waste

plastics. *Nat Rev Methods Primers.* 2023;3(1):44.

doi: 10.1038/s43586-023-00227-w

6. Wu X, Liu X, Song Y, *et al*. A Minimalist Design for a Dual-Catalyst System for High-Efficiency Conversion of Waste Plastics into Liquid Fuel Products. *J Am Chem Soc.* 2025;147(25):21907-21915.

doi: 10.1021/jacs.5c05246

7. Chea JD, Yenkie KM, Stanzione III JF, Ruiz-Mercado GJ. A generic scenario analysis of end-of-life plastic management: Chemical additives. *J Hazard Mater*. 2023;441:129902.

doi: 10.1016/j.jhazmat.2022.129902

8. Pottinger AS, Geyer R, Biyani N, *et al*. Pathways to reduce global plastic waste mismanagement and greenhouse gas emissions by 2050. *Science*. 2024;386(6726):1168-1173.

doi: 10.1126/science.adr3837

9. Yang Y, Qiu J, Zhang H, He P, Lü F. How soon will landfilled plastics integrate into the geological carbon cycle? *Environ Sci Ecotechnol*. 2025;26:100590.

doi: 10.1016/j.ese.2025.100590

10. Żukowski W, Jankowski D, Baron J, Wrona J. Combustion dynamics of polymer wastes in a bubbling fluidized bed. *J Clean Prod*. 2021;320:128807.

doi: 10.1016/j.jclepro.2021.128807

11. Chen Y, Awasthi AK, Wei F, Tan Q, Li J. Single-use plastics: Production, usage, disposal, and adverse impacts. *Sci Total Environ.* 2021;752:141772.

doi: 10.1016/j.scitotenv.2020.141772

12. Velis CA, Cook E. Mismanagement of plastic waste through open burning with emphasis on the global south: a systematic review of risks to occupational and public health. *Environ Sci Technol.* 2021;55(11):7186-7207.

doi: 10.1021/acs.est.0c08536

13. Zhou Q, Luo X, Gao X, *et al*. Impact of psychological distance on public acceptance of waste-to-energy combustion projects. *Environ Impact Assess Rev.* 2024;109:107631.

doi: 10.1016/j.eiar.2024.107631

14. Xu S, Li H, Wang Y, *et al*. Effect of chlorides on the melting behavior of municipal solid waste incineration fly ash. *J Environ Chem Eng.* 2025;13(2):116009.

doi: 10.1016/j.jece.2025.116009

15. Deng QX, Feng JR, Gao PP, Ni HG. Combined effects of vehicles and waste incineration on urban air halogenated and parent polycyclic aromatic hydrocarbons. *Environ Int*. 2023;171:107720.

doi: 10.1016/j.envint.2022.107720

16. Oluwoye I, Zeng Z, Mosallanejad S, Altarawneh M, Gore J, Dlugogorski BZ. Controlling NO*x* emission from boilers using waste polyethylene as reburning fuel. *Chem Eng J*. 2021;411:128427.

doi: 10.1016/j.cej.2021.128427

17. Zeng M, Ge Z, Wu Y, *et al*. Energy utilization of takeaway waste: Components separation and fuel preparation employing hydrothermal carbonization and gasification. *Energy*. 2024;299:131426.

doi: 10.1016/j.energy.2024.131426

18. Olhan S, Antil B, Behera BK. Repair technologies for structural polymeric composites: An automotive perspective. *Compos Struct*. 2025;352(3):118711.

doi: 10.1016/j.compstruct.2024.118711

19. Kai X, Li R, Yang T, Shen S, Ji Q, Zhang T. Study on the co-pyrolysis of rice straw and high-density polyethylene blends using TG-FTIR-MS. *Energy Convers Manag*. 2017;146:20-33.

doi: 10.1016/j.enconman.2017.05.026

20. Qin L, Han J, Zhao B, Wang Y, Chen WS, Xing FT. Thermal degradation of medical plastic waste by in-situ FTIR, TG-MS, and TG-GC/MS coupled analyses. *J Anal Appl Pyrolysis*. 2018;136:132-145.

doi: 10.1016/j.jaap.2018.10.012

21. Liu X, Tian K, Chen Z, Wei W, Xu B, Ni BJ. Online TG-FTIR-MS analysis of the catalytic pyrolysis of polyethylene and polyvinyl chloride microplastics. *J Hazard Mater*. 2023;441(5):129881.

doi: 10.1016/j.jhazmat.2022.129881

22. Wang X, Tang S, Ding L, *et al*. Contribution of plastic solid components to volatile organic compounds formation during plastics combustion. *J Hazard Mater*. 2024;480:135977.

doi: 10.1016/j.jhazmat.2024.135977

23. Li Y, Pöschl U, Shiraiwa M. Molecular corridors and parameterizations of volatility in the chemical evolution of organic aerosols. *Atmos Chem Phys*. 2016;16(5):3327-3344.

doi: 10.5194/acp-16-3327-2016

24. Kroll JH, Donahue NM, Jimenez JL, *et al*. Carbon oxidation state as a metric for describing the chemistry of atmospheric organic aerosol. *Nat Chem*. 2011;3(2):133-139.

doi: 10.1038/nchem.948

25. Wu X, Chen X, Jiang R, You J, Ouyang G. New insights into the photo-degraded polystyrene microplastic: Effect on the release of volatile organic compounds. *J Hazard Mater*. 2022;431:128523.

doi: 10.1016/j.jhazmat.2022.128523

26. Qiu Y, Zhong W, Shao Y, Yu A. Reactive force field molecular dynamics (ReaxFF MD) simulation of coal oxy-fuel combustion. *Powder Technol*. 2020;361:337-348.

doi: 10.1016/j.powtec.2019.07.103

27. Feng Y, Hao H, Chow CL, Lau, D. Exploring reaction mechanisms and kinetics of cellulose combustion via ReaxFF molecular dynamics simulations. *Chem Eng J*. 2024;488:151023.

doi: 10.1016/j.cej.2024.151023

28. Yu X, Chen J, Meng X, *et al*. Polyethylene deflagration characterization and kinetic mechanism analysis. *Energy*. 2024;303:131990.

doi: 10.1016/j.energy.2024.131990

29. Saha T, Bhowmick AK, Oda T, Miyauchi, T., Fujii, N. Understanding thermo-oxidative degradation of polyacrylic ester elastomer and its nanocomposites through molecular dynamics simulation and experiments. *Polym Degrad Stab*. 2021;183:109457.

doi: 10.1016/j.polymdegradstab.2020.109457

30. Hong D, Guo X. Molecular dynamics simulations of Zhundong coal pyrolysis using reactive force field. *Fuel*. 2017;210:58-66.

doi: 10.1016/j.fuel.2017.08.061

31. Xu F, Liu H, Wang Q, *et al*. ReaxFF-based molecular dynamics simulation of the initial pyrolysis mechanism of lignite. *Fuel Process Technol*. 2019;195:106147.

doi: 10.1016/j.fuproc.2019.106147

32. Ji J, Zhu W. Thermal decomposition of core–shell structured HMX@ Al nanoparticle simulated by reactive molecular dynamics. *Comput Mater Sci*. 2022;209:111405.

doi: 10.1016/j.commatsci.2022.111405

33. Song F, Li T, Zhang J, *et al*. Novel insights into the kinetics, evolved gases, and mechanisms for biomass (sugar cane residue) pyrolysis. *Environ Sci Technol*. 2019;53(22):13495-13505.

doi: 10.1021/acs.est.9b04595

34. Song F, Li T, Shi Q, *et al*. Novel insights into the molecular-level mechanism linking the chemical diversity and copper binding heterogeneity of biochar-derived dissolved black carbon and dissolved organic matter. *Environ Sci Technol*. 2021;55(17):11624-11636.

doi: 10.1021/acs.est.1c00083

35. Hur J, Jung KY, Jung YM. Characterization of spectral responses of humic substances upon UV irradiation using two-dimensional correlation spectroscopy. *Water Res*. 2011;45(9):2965-2974.

doi: 10.1016/j.watres.2011.03.013

36. Park Y, Jin S, Park E, *et al*. Chemical images and 2D-COS analysis of spin-coated PHBH*x*/PEG blend films. *J Mol Struct*. 2020;1216:128344.

doi: 10.1016/j.molstruc.2020.128344

37. Noda I. Close-up view on the inner workings of two-dimensional correlation spectroscopy. *Vib Spectrosc*. 2012;60:146-153.

doi: 10.1016/j.vibspec.2012.01.006

38. Chen W, Teng CY, Qian C, Yu HQ. Characterizing properties and environmental behaviors of dissolved organic matter using two-dimensional correlation spectroscopic analysis. *Environ Sci Technol*. 2019;53(9):4683-4694.

doi: 10.1021/acs.est.9b01103

39. Peng BY, Wang WX. In Vivo visualization of microplastic degradability and intestinal functional responses in a plastivore insect. *J Hazard Mater*. 2025;486:137109.

doi: 10.1016/j.jhazmat.2025.137109

40. Kissinger HE. Variation of peak temperature with heating rate in differential thermal analysis. *J Res Natl Bur Stand*. 1956;57(4):217-221.

doi: 10.6028/jres.057.026

41. Ozawa T, Isozaki H, Negishi A. A new type of quantitative differential thermal analysis. *Thermochim Acta*. 1970;1(6):545-553.

doi: 10.1016/0040-6031(70)80006-5

42. Starink MJ. A new method for the derivation of activation energies from experiments performed at constant heating rate. *Thermochim Acta*. 1996;288(1-2):97-104.

doi: 10.1016/S0040-6031(96)03053-5

43. Dewapriya MAN, Miller RE. Quantum and classical molecular dynamics simulations of shocked polyurea and polyurethane. *Comput Mater Sci*. 2022;203:111166.

doi: 10.1016/j.commatsci.2021.111166

44. Wood MA, Van Duin ACT, Strachan A. Coupled thermal and electromagnetic induced decomposition in the molecular explosive αHMX; a reactive molecular dynamics study. *J Phys Chem A*. 2014;118(5):885-895.

doi: 10.1021/jp406248m

45. Li W, Yu S, Zhang L, Chen J, Cao W, Lan Y. ReaxFF molecular dynamics simulations of n-eicosane reaction mechanisms during pyrolysis and combustion. *Int J Hydrog Energy*. 2021;46(78):38854-38870.

doi: 10.1016/j.ijhydene.2021.08.234

46. Batuer, A, Chen, D, He, X, Huang Z. Simulation methods of cotton pyrolysis based on ReaxFF and the influence of volatile removal ratio on volatile evolution and char formation. *Chem Eng J*. 2021;405:126633.

doi: 10.1016/j.cej.2020.126633

47. Bhoi S, Banerjee T, Mohanty K. Molecular dynamic simulation of spontaneous combustion and pyrolysis of brown coal using ReaxFF. *Fuel*. 2014;136:326-333.

doi: 10.1016/j.fuel.2014.07.058

48. Chen R, Lu S, Zhang Y, Lo, S. Pyrolysis study of waste cable hose with thermogravimetry/Fourier transform infrared/ mass spectrometry analysis. *Energy Convers Manag.* 2017;153:83-92.

doi: 10.1016/j.enconman.2017.09.071

49. Xu G, Cai X, Wang L, *et al*. Thermogravimetric-infrared analysis and performance optimization of co-pyrolysis of oily sludge and rice husks. *Int J Hydrog Energy.* 2022;47(64):27437-27451.

doi: 10.1016/j.ijhydene.2022.06.099

50. Nel HA, Chetwynd AJ, Kelly CA, *et al*. An untargeted thermogravimetric analysis-fourier transform infrared-gas chromatography-mass spectrometry approach for plastic polymer identification. *Environ Sci Technol*. 2021;55(13):8721-8729.

doi: 10.1021/acs.est.1c01085

51. Hong D, Gao P, Wang C. A comprehensive understanding of the synergistic effect during co-pyrolysis of polyvinyl chloride (PVC) and coal. *Energy.* 2022;239:122258.

doi: 10.1016/j.energy.2021.122258

52. de la Fuente AM, Marhuenda-Egea FC, Ros M, *et al*. Thermogravimetry coupled with mass spectrometry was successfully used to quantify polyethylene and polystyrene microplastics in organic amendments. *Environ Res*. 2022;213:113583.

doi: 10.1016/j.envres.2022.113583

53. Wang G, Li D, Yuan X, *et al*. Co-hydrothermal carbonization of polyvinyl chloride and pyrolysis carbon black for the preparation of clean solid fuels. *Fuel.* 2024;361:130550.

doi: 10.1016/j.fuel.2023.130550

54. Huo Y, Guo Z, Li Q, *et al*. Chemical fingerprinting of HULIS in particulate matters emitted from residential coal and biomass combustion. *Environ Sci Technol*. 2021;55(6):3593-3603.

doi: 10.1021/acs.est.0c08518

55. Lu Q, Zhao Y, Robinson AL. Comprehensive organic emission profiles for gasoline, diesel, and gas-turbine engines including intermediate and semi-volatile organic compound emissions. *Atmos Chem Phys.* 2018;18(23):17637-17654.

doi: 10.5194/acp-18-17637-2018

56. Zhao Y, Saleh R, Saliba G, *et al*. Reducing secondary organic aerosol formation from gasoline vehicle exhaust. *Proc Natl Acad Sci USA*. 2017;114(27):6984-6989.

doi: 10.1073/pnas.1620911114

57. Liu M, Han B, Bai J, *et al*. Insights into the co-combustion characteristics and synergistic effects of biomass and polyethylene plastic under rapid heating conditions. *Energy.* 2025;325:136113.

doi: 10.1016/j.energy.2025.136113

58. Zeng G, Su Y, Jiang J, Huang Z. Nitrogenative Degradation of Polystyrene Waste. *J Am Chem Soc*. 2025;147(3):2737-2746.

doi: 10.1021/jacs.4c15500

59. Han H, Yan P, Li Q, *et al*. Photothermal upcycling of waste polyvinyl chloride plastics. *Environ Sci Technol.* 2024;58(49):21861-21870.

doi: 10.1021/acs.est.4c07350

60. Jiang Q, Zhao Y, Zhang C, Yang J, Wang D. Investigation on the overlapping bands of syndiotactic polystyrene by using 2D-IR spectroscopy. *J Mol Struct.* 2016;1124:98-102.

doi: 10.1016/j.molstruc.2016.03.103

61. Song F, Li T, Wu F, Leung KMY, Bai Y, Zhao X. Dynamic evolution and covariant response mechanism of volatile organic compounds and residual functional groups during the online pyrolysis of coal and biomass fuels. *Environ Sci Technol.* 2022;56(9):5409-5420.

doi: 10.1021/acs.est.1c08400

62. Panahi-Sarmad M, Kasbi SF, Shojaei S, *et al*. Influence of polypropylene and nanoclay on thermal and thermo-oxidative degradation of poly (lactide acid): TG-FTIR, TG-DSC studies and kinetic analysis. *Thermochim Acta*. 2020;691:178709.

doi: 10.1016/j.tca.2020.178709

63. Gao Q, Ni L, Rong S, *et al*. Disposal of bamboo-based plastic substitute waste: A case study on co-pyrolysis and co-combustion of bamboo and polylactic acid. *Energy*. 2025;329:136822.

doi: 10.1016/j.energy.2025.136822

64. Chaudhuri P, Pande R, Baraiya NA. From char to flame: Evaluating bamboo bio-char combustion via cone calorimetry and thermogravimetric analysis. *Energy*. 2025;314:134313.

doi: 10.1016/j.energy.2024.134313

65. Zhang Y, Zhang C, Li W, *et al*. Reaction mechanism of stearic acid pyrolysis via reactive molecular dynamics simulation and TG-IR technology. *Renew Energy.* 2023;217:119115.

doi: 10.1016/j.renene.2023.119115

66. Li W, Zhang X, Liu R, *et al*. Thermal decomposition, flame propagation, and combustion reactions behaviours of stearic acid by experiments and molecular dynamic simulation. *Chem Eng J*. 2023;461:141906.

doi: 10.1016/j.cej.2023.141906

67. Ganguly S, Das P, Banerjee S, Das NC. Advancement in science and technology of carbon dot-polymer hybrid composites: A review. *Funct Compos Struct*. 2019;1(2):022001.

doi: 10.1088/2631-6331/ab0c80

68. Deng T, Chen Y, Hou D. Practically simple, catalyst-free, and scalable approach for all-component upcycling of mixed PVC/PA plastics. *Waste Manag*. 2025;205:115002.

doi: 10.1016/j.wasman.2025.115002